JACS
JOURNAL OF THE AMERICAN CHEMICAL SOCIETY
Article
pubs.acs.org/JACS

Proton-Coupled Electron Transfer Dynamics in the Catalytic Mechanism of a [NiFe]-Hydrogenase

Brandon L. Greene,[†] Chang-Hao Wu,[‡] Patrick M. McTernan,[‡] Michael W. W. Adams,[‡] and R. Brian Dyer*[,†]

[†]Chemistry Department, Emory University, Atlanta, Georgia 30322, United States
[‡]Department of Biochemistry, University of Georgia, Athens, Georgia 30602, United States

Supporting Information

ABSTRACT: The movement of protons and electrons is common to the synthesis of all chemical fuels such as H_2. Hydrogenases, which catalyze the reversible reduction of protons, necessitate transport and reactivity between protons and electrons, but a detailed mechanism has thus far been elusive. Here, we use a phototriggered chemical potential jump method to rapidly initiate the proton reduction activity of a [NiFe] hydrogenase. Coupling the photochemical initiation approach to nanosecond transient infrared and visible absorbance spectroscopy afforded direct observation of interfacial electron transfer and active site chemistry. Tuning of intramolecular proton transport by pH and isotopic substitution revealed distinct concerted and stepwise proton-coupled electron transfer mechanisms in catalysis. The observed heterogeneity in the two sequential proton-associated reduction processes suggests a highly engineered protein environment modulating catalysis and implicates three new reaction intermediates; Ni_a-I, Ni_a-D, and Ni_a-SR^-. The results establish an elementary mechanistic understanding of catalysis in a [NiFe] hydrogenase with implications in enzymatic proton-coupled electron transfer and biomimetic catalyst design.

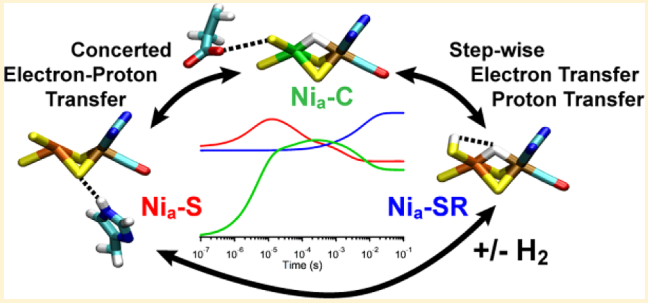

INTRODUCTION

All chemical reactions involve the movement of electrons, and most additionally involve the movement of protons as a means of maintaining electroneutrality. It has been shown that the movement of these fundamental particles can be coupled into a single chemical step, concerted electron−proton transfer (EPT), which can be advantageous thermodynamically.[1,2] In biological systems such as enzymes, electrons and protons often traverse different pathways through the protein. Despite this spatial separation (multi-site EPT, MS-EPT), the protein matrix has been proposed to modulate EPT through static and dynamic properties that are not completely understood.[2−7]

Proton transfer (PT), electron transfer (ET), and EPT are processes of particular importance in oxidoreductases due to their obligatory involvement of protons and electrons for reactivity. Hydrogenases (H_2ases), oxidoreductases that catalyze the reversible oxidation of H_2, require multiple protons and electrons to be transported over large distances and eventually combined.[8,9] These enzymes are remarkably efficient, with high turnover frequencies (TOF) and low overpotentials that rival platinum, but contain nonprecious bimetallic active sites composed of nickel and/or iron.[10,11] As a result, hydrogenases have stimulated substantial research in biotechnological applications and biomimetic analogues.[12−17]

The [NiFe] H_2ases have been the most studied of these enzymes, and a rudimentary mechanism has been proposed based on numerous studies of steady state behavior (Scheme 1).[9,18,19] The current mechanistic understanding of [NiFe] H_2ases is based on three equilibrium states denoted Ni_a-S, Ni_a-C, and Ni_a-SR which react with or result from reactions with H_2.[20,21] These states are separated by two sequential proton-coupled n = 1 reductions, but their spectroscopic properties indicate that these two processes are inequivalent.[22−26] The first proton-associated reduction, conversion of Ni_a-S to Ni_a-C, results in the formation of a metal bridging hydride, a two electron reduced proton, with the additional electron being donated by nickel. The storage of electrons on the ligand in the form of a hydride aids in leveling the redox transitions of the active site, analogous to the reductive chemistry of the nitrogenases.[27] The second reduction event, conversion of Ni_a-C to Ni_a-SR, results in a reduced nickel center and the protonation of a terminal cysteine ligand to the nickel.[28] The origin of this heterogeneity and the details of the proton-coupled transitions are still debated thus the mechanism as it stands is incomplete. Furthermore, no study to date has examined the catalytic intermediate transitions on time scales faster than the TOF, thus their involvement in the mechanism is an open question.[19−21]

Herein we use a phototriggered chemical potential jump method to initiate redox chemistry by a [NiFe] H_2ase from *Pyrococcus furiosus* (*Pf*) on the sub-TOF time scale. Coupling

Received: February 17, 2015
Published: March 19, 2015

DOI: 10.1021/jacs.5b01791
J. Am. Chem. Soc. 2015, 137, 4558−4566

Scheme 1. Representative Structure and Function of the [NiFe] H_2ases[a]

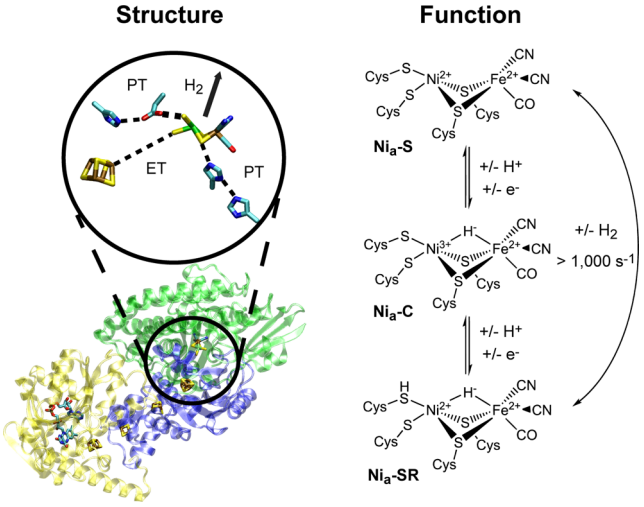

[a]Crystal structure of the type III [NiFe] H_2ase from *Methanothermobacter marburgensis* (PDB code 4OMF) with expanded view of the active site, proton (PT) and electron transfer (ET) networks near the active site (Structure) and current mechanistic proposal for H_2ase activity (Function). Coloring scheme: carbon, cyan; nitrogen, blue; oxygen, red; sulfur, yellow; iron, brown; nickel, green. Dotted lines represent proposed ET and PT pathways.

this phototriggering method to nanosecond time-resolved infrared spectroscopy enabled direct observation of the active site chemistry after photolysis. The kinetic data yielded new chemical insight into the mechanism of this enzyme, revealing a critical role of EPT and new intermediates previously inaccessible.

EXPERIMENTAL METHODS

***Pf* H_2ase Preparation.** *Pf* growth, soluble hydrogenase I (SHI) expression and purification were performed without modification from a recently developed protocol for nickel–NTA affinity chromatographic purification of a histidine tagged version of SHI.[29] Purified protein was stored anaerobically under 5% H_2 in 2 mM DTT, 300 mM NaCl, and 50 mM Tris buffer pH = 7.0.

Steady State Kinetics. Steady state kinetics for H_2 production by the *Pf* H_2ase was measured by gas chromatography (GC). The GC measurements were calibrated by performing controlled injections of H_2 under identical liquid and gas headspace volumes. With the use of the known density of H_2 at NTP, the integrated peak area was calibrated to H_2 content in the headspace. This was repeated with D_2 gas (for kinetic isotope effect (KIE) measurements), which gave similar results for the calibration curve.

H_2ase steady state kinetics samples (20 nM) were prepared in buffers (50 mM PO_4 at appropriate pH(D)) containing 5% H_2 in an N_2 atmosphere. After preparation, the samples were flushed with pure N_2 for 15 min under vigorous stirring. Samples were subsequently allowed to equilibrate for another 10 min after which the headspace was analyzed to confirm the removal of H_2. Next a concentrated stock solution of methyl viologen (MV) and $Na_2S_2O_4$ was injected to a final concentration of 5 mM MV and 10 mM $Na_2S_2O_4$, initiating the timing of the kinetics experiment. Samples of the headspace were measured every 5 min and experiments were repeated at least three times with error reported as the standard deviation of the measurements at each time point.

For the β-nicotinamide adenine dinucleotide (NADH) photolysis driven H_2 production assay, 200 μM NADH, 10 mM MV^{2+} and 20 nM H_2ase were mixed in 50 mM PO_4 buffer pH 7.0. The sample was illuminated by a 351 nm Nd:YLF laser (Crystalaser, Inc.) at 50 mW incident power, a repetition rate of 2 kHz and focused to 500 μm diameter spot through the 1 cm path of the cuvette.

Nanosecond Kinetics Sample Preparation. Samples for transient experiments were prepared as follows. Solutions of 2 mg of active *Pf* H_2ase were exchanged into 10 mM MV^{2+} and 50 mM phosphate with pH(D) values of 6.3, 7.0, and 7.7 by 50 kDa molecular weight cutoff centrifugal filters (Millipore) under an H_2 free atmosphere until no further H_2 induced MV^{2+} reduction was observed. This protocol prepared the various enzyme samples in similar equilibrium state distributions and under slightly oxidized conditions amenable to photoreduction. Deuterated buffers were initially prepared in H_2O identically, then subsequently freeze-dried and redissolved into pure D_2O (99.9%, Cambridge Isotopes, Inc.) twice. The MV^{2+} exchanged *Pf* SHI samples were then exchanged similarly into 12 mM NADH, 10 mM MV^{2+} and 50 mM phosphate at the appropriate pH(D) and concentrated to a final volume of 10–15 μL resulting in a final concentration of 1.5 mM H_2ase based on a molecular weight of 153 000 Da. The concentrated sample was loaded into one-half of a split infrared transmission cell employing CaF_2 windows sandwiching a dividing Teflon spacer (path length = 75 μm) and sealed. The reference was prepared similarly except for the use of reduced horse heart myoglobin (deoxyMb) at a concentration of 2 mM Mb which matched the optical density at 355 nm (Supporting Information Figure S1).

Fourier Transform Infrared Spectroscopy (FTIR) Characterization. FTIR spectra were measured on samples used for transient measurements with an MCT equipped Varian Excalibur FTIR spectrometer. Samples were maintained at 20 °C via a recirculating water bath. Reported spectra represent the average of 1024 scans at 2 cm^{-1} resolution and were baseline corrected with a multipoint spline function, which corrected for the substantial difference in protein to H_2O/D_2O ratio between sample and reference.

Simultaneous Transient Visible/Infrared Absorption Spectroscopy. Instrumental design of the simultaneous transient infrared/visible absorption system are described in detail in the Supporting Information (Figure S2). Transient visible and infrared spectra were collected at room temperature using 150 μJ of 355 nm light focused to a 200 μm diameter spot (500 mJ/cm^2). Samples were rastered between pulses to ensure a unique sample spot was being probed every pulse and 50 shots were averaged for every probed wavelength. Transient signals were ratioed to the unpumped probe intensity to generate a ΔA after time zero, then the solvent thermal signal (2–3 °C temperature jump due to nonradiative relaxation of pump energy) was subtracted via the deoxyMb reference infrared data yielding the reported $\Delta\Delta A$ (Supporting Information Figure S5).

Data Analysis. The transient data were fit using IGOR software (WaveMetrics, Inc.) to a model shown pictorially in the inset of Figure 3. Briefly, the Ni_a-S and Ni_a-C state transitions were fit by two coupled exponential functions which represent the concerted conversion of Ni_a-S to Ni_a-C by solvated electrons and MV^+ with two different pseudo-first order rates. The Ni_a-C and Ni_a-S states were reformed from Ni-L by concerted processes as well, fit to two Ni-L coupled rates. Finally, the Ni_a-C to Ni_a-SR conversion was modeled as two uncoupled processes (Supporting Information Figure S6, Table S4). Thus, the global fitting consisted of four coupled rates (2× Ni_a-S to Ni_a-C, Ni-L to Ni_a-C and Ni-L to Ni_a-S) and two uncoupled rates (Ni_a-C bleach and Ni_a-SR formation).

RESULTS AND DISCUSSION

The soluble hydrogenase I (SHI) from the hyperthermophile *Pf* is a type 3 [NiFe] H_2ase involved in H_2 oxidation coupled to $NADP^+$ reduction.[30,31] This enzyme is a heterotetramer consisting of two "standard" subunits harboring the [NiFe] active site and a three Fe_4S_4 iron sulfur cluster chain respectively, as well as two additional subunits containing Fe_4S_4 and Fe_2S_2 clusters and a flavin cofactor which function in native cofactor ($NADP^+$) binding and reduction.[30,32] The *Pf* SHI enzyme has previously been characterized by electron paramagnetic resonance spectroscopy (EPR), FTIR, and X-ray

DOI: 10.1021/jacs.5b01791
J. Am. Chem. Soc. 2015, 137, 4558–4566

absorbance spectroscopy (XAS) spectroscopy, in addition to numerous kinetic and biochemical studies and has been shown to exhibit similar spectroscopic and reactive properties to other known [NiFe] H_2ases from various microorganisms and types (Supporting Information).[30−35]

Infrared Spectroscopy of *Pf* SHI. Infrared spectroscopy is well established for the study of H_2ase, utilizing the intrinsic CO and CN ligands of the active site iron, which report on the electronic structure of the active site irrespective of oxidation state.[22,25,36] The CO and CN vibrational spectra of the *Pf* H_2ase (Figure 1b) are highly sensitive to the applied chemical or electrochemical potential, and analogously to pH as has been observed in other [NiFe] H_2ases.[20,22−25] The vibrational spectrum of the *Pf* SHI shows a distribution of CO vibrational resonances associated with equilibrium states under mildly reducing conditions, consistent with previous studies (Figure 1a).[34] Multipeak fitting of the CO region based on second derivative analysis, oxidative treatment, pH dependence, difference spectra and literature precedence (Figure 1a,b , Supporting Information Figure S3 and Table S1) revealed peaks consistent with the known equilibrium states; Ni_a-S (1950 cm^{-1}), Ni_a-C (1967 cm^{-1}), Ni_a-SR (1954 cm^{-1}) and additional peaks we tentatively assign to the Ni_a-SR(′) (1940 cm^{-1}) and Ni_a-SR(″) (1931 cm^{-1}) states (Supporting Information). The interconversion among these states is subsequently examined by time-resolved infrared spectroscopy following a phototriggered perturbation of the system reduction potential at the infrared frequencies indicated by colored arrows in Figure 1a.

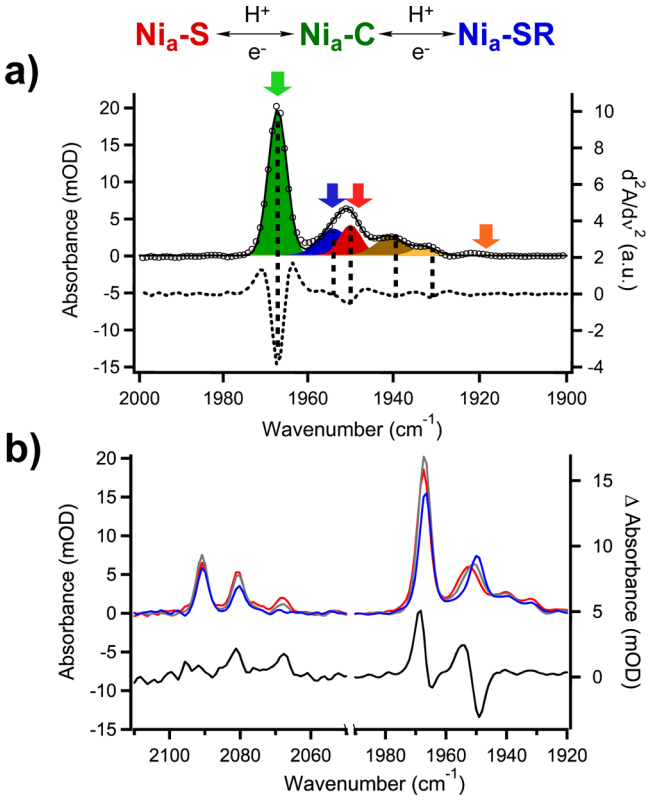

Figure 1. FTIR spectra of the *Pf* SHI. (a) Multipeak Gaussian fitting to experimental data for the CO absorbance region of *Pf* SHI at pH 7.0 based on second derivative analysis, oxidative treatment and previous reports. Open circles, experimental data; solid black line, multi-Gaussian fit; colored peaks, multi-Gaussian fit components (left ordinate); dotted line, second derivative of experimental data (right ordinate). Vertical lines show peak correlation in experimental and second derivative data. (b) pH dependence of the CO and CN FTIR signals and difference spectrum for low pH minus high pH data. Colors: blue, pH 7.7; gray, pH 7.0, red pH 6.3 (left ordinate), and black pH 6.3−7.7 (right ordinate).

Laser-Induced Chemical Potential Jump. The proton reduction TOF of 62 s^{-1} for *Pf* SHI at room temperature (Supporting Information Figure S4) necessitates fast (≤ms) proton and electron transfer to facilitate catalysis. Consequently, methods of rapidly initiating the reactivity of the enzyme are critical to observe these processes directly. In pursuit of such a rapid initiation method, we implemented a "caged electron" reagent, NADH, to phototrigger the reductive chemistry of the SHI using a pulsed laser as an optical trigger, stimulating photoionization of NADH to produce a solvated electron and $NADH^{+\bullet}$ cation radical on the nanosecond time scale.[37−39] To validate this method and confirm that it is capable of stimulating enzymatic turnover, we examined H_2ase derived photocatalytic H_2 production by NADH photoionization in the presence of methyl viologen (MV), a functional redox mediator.[30]

Figure 2a shows the photocatalytic H_2 production by the *Pf* H_2ase after illumination by 355 nm light. Solvated electrons produced in the initial photoionization process were capable of turning over the enzyme, which is evident from the small amount of H_2 formed from NADH photolysis in the absence of MV^{2+}, but significant improvement in efficiency was observed

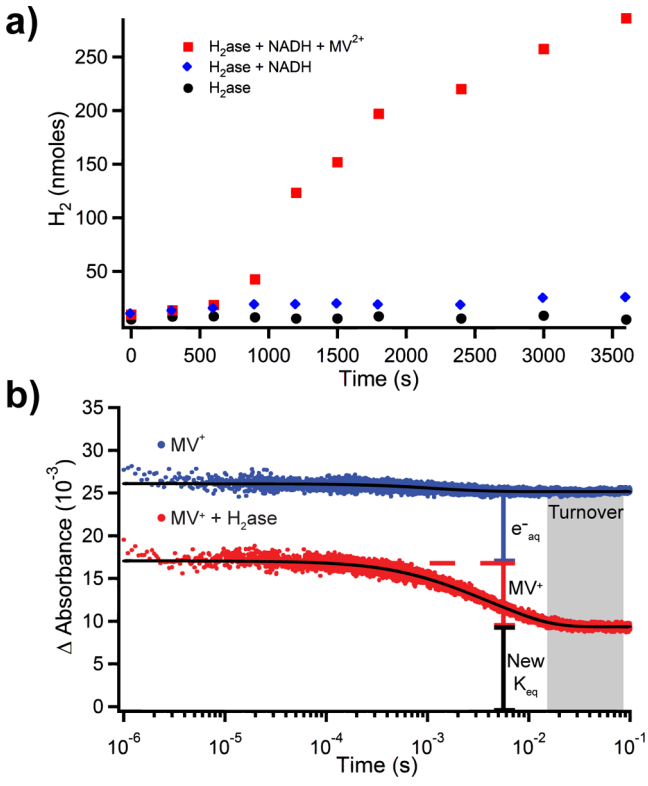

Figure 2. Photocatalysis and interfacial ET after photoionization of NADH. (a) Photocatalytic H_2 yield for H_2ase alone (black circles), H_2ase and NADH (blue diamonds), and H_2ase with MV^{2+} and NADH (red squares). (b) Transient visible data probed at 635 nm after photolysis for deoxyMb (blue) and SHI (red) with associated exponential fits (black).

DOI: 10.1021/jacs.5b01791
J. Am. Chem. Soc. 2015, 137, 4558−4566

over long time periods by the inclusion of MV^{2+}. The activity of the *Pf* SHI was measured before and after bulk photocatalysis, which showed a 48% loss in activity (Supporting Information Figure S7). This may be due to enzyme degradation due to the laser illumination, reactions with photoionization products, poor enzyme recovery or diminished activity over 10^5 turnovers.

To confirm sub-TOF intermolecular ET, we used transient visible absorbance sensitive to the MV^+ radical photoproduct (Figure 2b). In control experiments, photoionization of NADH resulted in the production of 530 μM MV^+ in the absence of the catalytic acceptor SHI (Supporting Information). This MV^+ concentration jump was capable of decreasing the equilibrium reduction potential in the cell by 50 mV (Supporting Information).

DeoxyMb was used in these control experiments as a protein-based UV absorber that did not interact with MV^+ to match the optical density at the pump wavelength relative to the H_2ase samples, thus matching the inner filter effect (Supporting Information Figure S1). The MV^+ signal decayed less than 5% over 100 ms post photolysis, confirming the anaerobic environment of the infrared (IR) cell. When SHI was present, dramatic differences in the initial absorbance and subsequent decay kinetics of MV^+ were observed (red trace Figure 2b). We attribute the initial absorbance difference to direct reduction of SHI by the solvated electron occurring faster than the experimental time resolution, which competes with MV^{2+} reduction. On the basis of the difference in MV^+ formation in the H_2ase samples relative to the deoxyMb samples, 200 μM of solvated electrons are consumed by SHI by intermolecular ET, presumably to an exposed redox cofactor, on a very rapid time scale (<100 ns). The subsequent decay of MV^+ was observed to be biphasic, with relaxation rates of 1.0×10^3 s^{-1} (40%) and 2.0×10^2 s^{-1} (60%) with a net consumption of 200 μM MV^+. We attribute the two phases to multiple ET sites on the enzyme surface with competitive, but different rates, such as the flavin or Fe_4S_4 cofactors.[30,32] These results demonstrate a cumulative reduction of 400 μM H_2ase (~27%) within ca. 5 ms, well below the enzymes TOF, approximately half of which occurs faster than the time resolution of the experiment. The equilibrium distributions of Ni_a-S, Ni_a-C and Ni_a-SR are expected to react with equal probability based on initial populations with the solvated electron, $NADH^{+\bullet}$ radical and MV^+; thus, active site dynamics unhindered by any other kinetic process should be observed on these time scales. After partial MV^+ oxidation, a new H_2ase mediated MV^+/MV^{2+} equilibrium was established, as demonstrated by the stable residual MV^+ absorbance which persisted with minimal diffusional decay for minutes. On the basis of the populations of Ni_a-S, Ni_a-C and Ni_a-SR, it is expected that most photoreduction results in enzyme reduction, but little H_2 is produced with these modest potential jumps below the H_2/H^+ couple. Thus, the interconversion of the equilibrium states could be examined by this method despite little overall turnover. FTIR spectra were collected before and after photolysis experiments (Supporting Information Figure S8), indicating negligible photodegradation during transient data collection. This result demonstrates that the photocatalysis induced activity loss is the result of enzyme degradation, not due to direct photodegradation.

Phototriggered SH1 Kinetics. Nanosecond transient infrared absorbance signals (Figure 3) from the steady states Ni_a-S, Ni_a-C, Ni_a-SR and the photoproduct Ni-L were collected

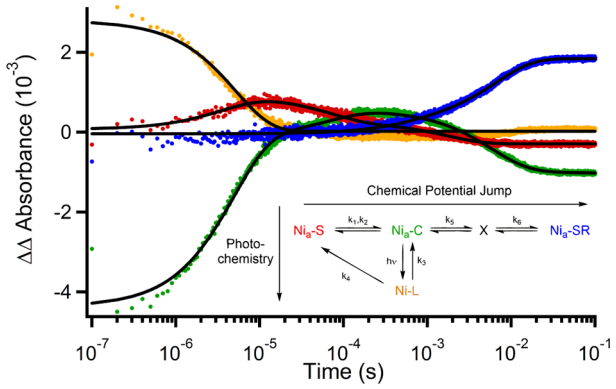

Figure 3. Transient infrared data probed at frequencies illustrated in Figure 1a. Color scheme: Ni_a-S (1948 cm^{-1}), red; Ni_a-C (1967 cm^{-1}), green; Ni-L (1920 cm^{-1}), orange; Ni_a-SR (1954 cm^{-1}), blue; global fits, black. Inset shows kinetic model used to fit the experimental data.

simultaneously with the visible transients at probe frequencies illustrated in Figure 1a. This was highly advantageous since interfacial ET and active site chemistry could be resolved under identical conditions at the same time, which substantially aided in the data interpretation. Dynamics for Ni_a-S, Ni_a-C and Ni_a-SR were observed within the overall TOF of the enzyme, the first direct evidence validating the kinetic competency of these proposed intermediates. Kinetic competency is crucial in determining the relevance of the observed equilibrium states in the catalytic cycle, eliminating their potential as off-pathway thermodynamic trap states.

Ni_a-S yielded transients displaying three phases (red trace in Figure 3). The earliest feature observed was an induced absorbance with a relaxation rate of $2.9 \pm 0.3 \times 10^5$ s^{-1}. We attributed this phase to the formation of Ni_a-S by ET (and possibly PT) from the photoproduct Ni-L state, a recently discovered phenomenon.[40] This process is the most direct measure of the ET rate between the proximal iron–sulfur cluster and the [NiFe] active site to date. This may aid in the experimental determination of the reorganization energy and wave function overlap in ET to the active site from the proximal Fe_4S_4 cluster, a common feature of all [NiFe] H_2ases. Subsequently, a biphasic decay with rates of $(1.8 \pm 0.2) \times 10^4$ s^{-1} (56%) and $(5.0 \pm 2.4) \times 10^2$ s^{-1} (44%) was observed yielding a net bleach of the Ni_a-S absorbance, verifying a shift of the system to lower potential.

The two bleach phases are attributed to reduction by solvated electrons and MV^+, respectively, based on the associated time scales and amplitudes. We observed a substantial lag phase between the interfacial reduction of the enzyme by the solvated electron (<100 ns) and the eventual reduction of the active site (>50 μs). This lag phase describes the time required for ET through the protein to the buried active site following intermolecular ET; the lifetime is reasonable since ET between the proximal iron–sulfur cluster and the active site occurs in 3.5 ± 0.4 μs (*vide supra*) and there are likely multiple intramolecular ET steps.

The transient signals of the Ni_a-C state yielded more complex dynamics (green trace of Figure 3), as expected for an intermediate state. Immediately after the photoionization pulse, a bleach of the Ni_a-C state was observed due to fast (unresolved) photolysis of the bridging hydride, which is proposed to bind as a proton to a nearby base, a well-known phenomenon in [NiFe] H_2ases.[41,42] The photolysis product Ni-

DOI: 10.1021/jacs.5b01791
J. Am. Chem. Soc. 2015, 137, 4558–4566

L relaxed back to the Ni_a-C state with a rate of $(1.94 \pm 0.14) \times 10^5$ s^{-1}. Further assignment of the photolytic production of the Ni-L state was performed in the absence of NADH (Figure 4),

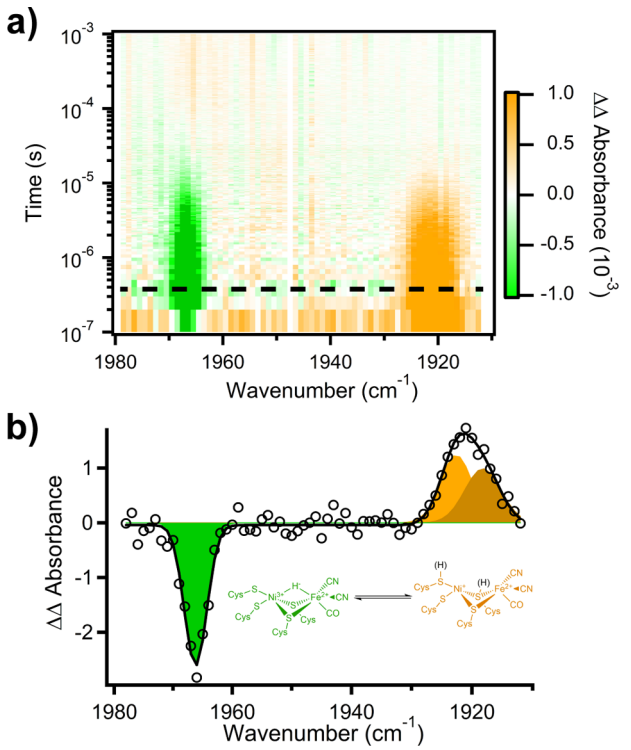

Figure 4. Transient infrared analysis of SHI photochemistry. (a) Transient infrared spectrum of SHI after photoexcitation with 355 nm light at 1 cm^{-1} resolution. (b) Transient infrared spectrum at 500 ns (dashed line in (a)). Circles represent experimental data, solid line represents multi-Gaussian fit, and colored peaks represent multi-Gaussian fit components. Inset shows active site structures of Ni_a-C and the photoproducts Ni-L with two potential proton acceptor sites.

in which two spectrally similar Ni-L states (1916 and 1923 cm^{-1}) were observed with very similar relaxation rates (2.0×10^5 and 1.4×10^5 s^{-1}, respectively, at pH 7.0). Multiple photoproduct states have been observed before and have been ascribed to different acceptor sites on the active site sulfur ligands.[43−47] The recovery of Ni_a-C from both Ni-L states were an order of magnitude faster than that predicted from cryogenic experiments for the H_2ase of *Desulfovibrio vulgaris* Miyazaki F.[42] This apparent discrepancy could be explained by a lowering of the activation barrier of the proton transfer step at room temperature due to the thermal mobility of an associated proton donor. This interpretation is corroborated by a smaller observed KIE (vide infra) of 2.8 relative to that observed at cryogenic temperatures of ca. 6.[42] An induced absorbance of the Ni_a-C transients was observed at intermediate time, concomitant and opposite in sign to the decay signal from Ni_a-S. We assign this process to the formation of Ni_a-C from Ni_a-S via a concerted mechanism. At later time, a bleaching of the Ni_a-C signal was observed with a rate of $(2.2 \pm 0.4) \times 10^2$ s^{-1} attributed to reduction of Ni_a-C to form Ni_a-SR. This 100-fold slower rate implies dissimilar mechanisms for the Ni_a-C state reduction relative to Ni_a-S reduction.

The most reduced active state, Ni_a-SR, also showed dynamics in our experiments with an induced absorbance at $(1.9 \pm 0.3) \times 10^2$ s^{-1} (blue trace, Figure 3). This was slightly delayed in time relative to the Ni_a-C state bleach indicating the presence of an intermediate, providing further evidence that the mechanisms of proton associated reduction of Ni_a-S and Ni_a-C are distinct. On the basis of independent kinetic analysis, a coupled kinetic model was applied described pictorially in the inset of Figure 3. The coupled model resulted in fits to the experimental data with similar but opposite amplitudes for transitions between connected states. Assuming similar oscillator strengths and a reasonable extinction coefficient of 1000 M^{-1} cm^{-1}, the total enzyme reduction was ca. 350 μM, which is again in agreement with the calculated electron transfer yield determined from the visible transient absorbance data.[48,49]

pH, Isotope, and Temperature Dependence of *Pf* SHI Kinetics. The methodology established above sets the stage for in depth investigation of the elementary mechanisms involved in PT, ET and active site chemistry. Little is known about key elements, including the overall rate-determining step(s), the effects of the protein matrix on ET and PT as well as the rates of active site chemistry relative to ET and PT. These details are critical in developing a complete understanding of the catalytic mechanism and may give rationale for the reversibility, bias and efficiency observed in these enzymes. Thus, to investigate the nature of proton and electron transfer in the conversion of Ni_a-S to Ni_a-C and Ni_a-C to Ni_a-SR, the transient experiments were reexamined at pH 7.0 and pH 7.7 as well as in D_2O (Figure 5). The steady state behavior under differing pH and solvent isotopes was also investigated for comparison to presteady state kinetics data.

(1). Ni_a-S to Ni_a-C and Ni-L to Ni_a-C Transitions. The concerted bleach of the Ni_a-S state and induced absorbance of the Ni_a-C state were highly pH dependent, with rates ranging from 2300 to 18 000 s^{-1} from pH 7.7 to 6.3. We conclude from these data that the conversion of Ni_a-S to Ni_a-C occurs through a concerted mechanism modulated by protonation of a donor residue near the active site with a pK_a near 7. The amplitudes of these features were also affected by pH with basic pH yielding the largest Ni_a-S bleach signals, consistent with initial Ni_a-S state content (Figure 1b, Supporting Information Table S2). This was corroborated by the observed Ni_a-C and Ni_a-SR state dynamics, which show a trend toward Ni_a-C state production over Ni_a-SR at higher pH, again consistent with the equilibrium concentrations of these species.

The nature of the concerted Ni_a-S to Ni_a-C transition was further examined by the H/D KIE. The KIE of concerted EPT processes is known to be unusually high ($k_H/k_D > 7$) in situations which involve an elementary electron−proton transfer reaction (proton and electron tunneling) due to the decrease in tunneling probability with the shortening of the de Broglie wavelength of the deuteron relative to the proton.[3] The kinetics of Ni_a-S reduction in H_2O and D_2O (Figure 5d) were drastically different. The KIE for Ni_a-S to Ni_a-C conversion was pH dependent and varied from 6 ± 1 to 43 ± 6 in the pH(D) range of 7.7−6.3, respectively (Supporting Information). The large KIE at acidic pH can only be reconciled by an EPT rate-determining step involving proton tunneling, whereas the basic KIE is more consistent with classical primary KIE process being rate determining. Additionally, in separate experiments, the activation barrier for the EPT process at pH 6.3, where the EPT mechanism is dominant, was determined to be 1.5 kcal/mol (Supporting Information Figure S9). This very low value is consistent with a fast, concerted EPT that is kinetically competitive with alternative ET and PT pathways. EPT is, in theory, pH independent. To rationalize the observed pH

DOI: 10.1021/jacs.5b01791
J. Am. Chem. Soc. 2015, 137, 4558−4566

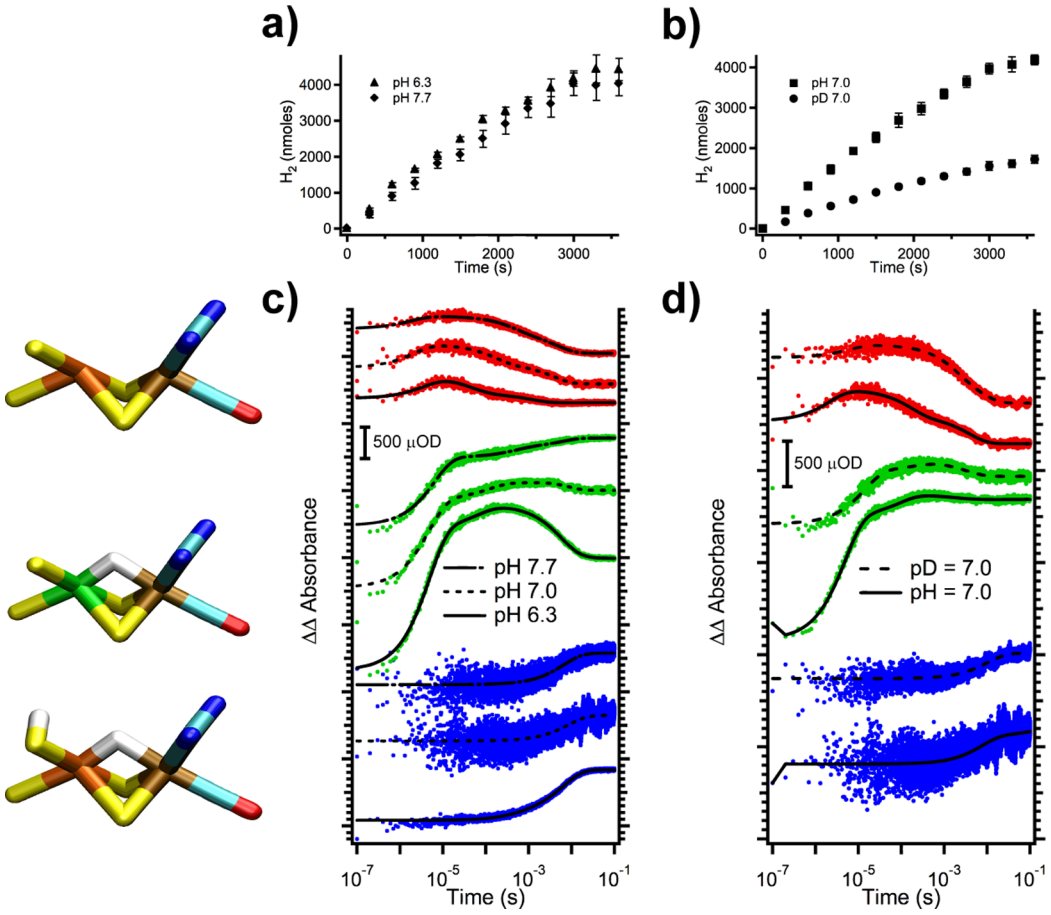

Figure 5. pH and solvent isotope effects on steady state and pre-steady state proton reduction kinetics. (a) H_2 production steady state kinetics at pH 7.7 (diamonds) and 6.3 (triangles). (b) H_2/D_2 production steady state kinetics at pH 7.0 (squares) and pD 7.0 (circles). (c) Transient infrared signatures for Ni_a-S (red), Ni_a-C (green) and Ni_a-SR (blue) with associated fits (black lines) at pH 7.7 (dotted dashed lines), 7.0 (dotted lines) and 6.3 (solid lines). (d) Transient infrared signatures for Ni_a-S (red), Ni_a-C (green) and Ni_a-SR (blue) with associated fits (black lines) at pH 7.0 (solid lines) and pD 7.0 (dotted lines). Structures of the [NiFe] active site in the various equilibrium redox states are visualized pictorally to the left of the associated transient data based on the recent structure of the [NiFe] H_2ase from *D. vulgaris* Miyazaki F (PDB 4U9H).[28]

dependence, we propose a simple kinetic model in which the EPT mechanism is gated by protonation of one or more ionizable amino acids in the protein. Since this reaction is fast relative to enzyme turnover, it is not expected to be reflected in the steady state data, which is clear from the minimal steady state KIE of 2.6 and the small pH dependence. This result highlights the substantial mechanistic insights obtained from sub-TOF kinetics experiments that are obscured by steady state measurements.

This is the first direct evidence for a MS-EPT mechanism in an enzyme as far as we are aware. In the MS-EPT mechanism, proton tunneling from an amino acid residue adjacent to the active site is coupled to long-range electron transfer from the proximal Fe_4S_4 cluster to the [NiFe] active site. This is distinct from the H atom transfer in soybean lipoxygenase where a proton and electron are transferred from a single bonding orbital.[4,50,51] The H atom transfer step in soybean lipoxygenase was observed to have a similarly low barrier (1.6 kcal/mol), but a much slower rate of 280 s^{-1}.[50,51] The Ni_a-S to Ni_a-C state transition necessarily involves proton and electron transfer as well as hydride formation. We observed no intermediate in this process, nor in the Ni-L recovery to Ni_a-C, which also involves proton transfer and subsequent hydride formation. Thus, the hydride formation chemical step must occur much faster (<50 μs) than the concerted EPT step. This reduced protonated state is involved in catalysis, but based on our measurements, could not be observed due to the slower EPT relative to hydride formation. We therefore term this state the Ni_a-I state based on its presence in the mechanism as a fleeting intermediate state en route to Ni_a-C state formation. This claim is supported by theoretical predictions where a reduced protonated state is predicted as an intermediate.[52−54] Importantly, our data also indicate that the Ni_a-I to Ni_a-C and Ni-L to Ni_a-C transitions are isoelectronically and isoprotically similar, and thus, the photochemical dynamics may be a rich model system for experimentally disentangling the hydride formation from the EPT process. On the basis of our observations of multiple Ni-L states at room temperature, it is likely that these states result in different proton binding sites upon hydride photolysis. Thus, the Ni_a-I state may in fact be identical to one of the observed Ni_a-L states allowing this kinetically obscured reaction intermediate to be studied more extensively.

The kinetics of Ni_a-S conversion to Ni_a-C in D_2O was also fit well to a concerted step, but showed little pH dependence. The $\log(k_{obs})$ versus pH plot for the Ni_a-S to Ni_a-C conversion in H_2O and D_2O (Figure 6) dramatically shows this difference. On the basis of the small pH dependence of the Ni_a-S to Ni_a-C conversion in D_2O, we propose that this process occurs through a PT-ET stepwise mechanism in which the active site is

DOI: 10.1021/jacs.5b01791
J. Am. Chem. Soc. 2015, 137, 4558−4566

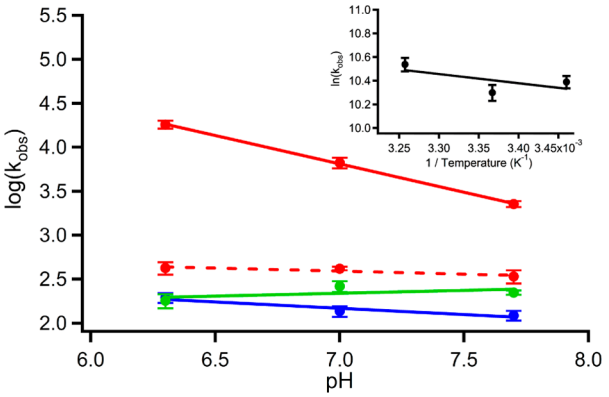

Figure 6. pH and temperature dependence of Ni_a-S, Ni_a-C and Ni_a-SR dynamics. The pH(D) dependence of the log(k_{obs}) for Ni_a-S reduction in H_2O (red solid line), D_2O (red dashed line), Ni_a-C reduction (green solid line) and Ni_a-SR formation (blue solid line). Inset shows the temperature dependence of the ln(k_{obs}) for Ni_a-S reduction.

protonated, followed by fast reduction to form the Ni_a-I state which subsequently forms the bridging hydride rapidly to finally form Ni_a-C. This PT-ET mechanism is intuitive because the reduction of the divalent nickel is a high energy species; thus, protonation of the active site would lower the electron density on the nickel facilitating reduction.

The difference in pH(D) dependence between the Ni_a-S to Ni_a-C transition in H_2O and D_2O suggests one of two possibilities; either proton transfer to the active site is slow relative to proton exchange of the donor residue (i.e., same donor in H_2O vs D_2O) or that there is a different proton donor residue entirely which facilitates the EPT process that is shut down upon deprotonation at pH > 7.7. On the basis of the large pH dependence of the KIE, we propose that it is pH that modulates PT from two different donors with different mechanisms, favoring the latter explanation. There are two potential proton donor residues, His^{75} and Glu^{17} (*Pf* H_2ase numbering), both of which are largely conserved in [NiFe] H_2ases and within H^+ tunneling distances to the active site cysteine ligands (Scheme 1). With the use of site directed mutagenesis and steady state kinetics, the glutamate residue has been shown to be critical in the enzymatic proton transport, but the histidine residue has been less explored.[55−57] We favor the histidine residue as the proton source for the EPT mechanism due to the observed pH dependence, consistent with a characteristic histidine pK_a. In the PT-ET mechanism, we favor the glutamic acid as the proton donor based on the dissimilarity in pH dependence relative to the EPT mechanism, site directed mutagenesis studies and theoretical predictions.[58]

[NiFe] hydrogenases typically function with high Michaelis constant (K_m) for H_2 and an electrochemically defined bias toward H_2 oxidation, despite almost no overpotential for the reversible reduction of protons.[59−62] The observed EPT mechanism reported for *Pf* [NiFe] H_2ase could potentially explain this bias, where a fast second proton coupled oxidation process pushes the equilibrium toward Ni_a-S in low H_2 conditions. Furthermore, it is interesting to note that the EPT mechanism only affects the Ni_a-S to Ni_a-C transition in the [NiFe] H_2ase, and has little kinetic effect in the proton reduction reaction since the formation of Ni_a-SR and subsequent product release are 100-fold slower. Others have shown multiple methods for kinetically tuning the bias of these enzymes through ET and H_2 diffusion, which together with the present results highlight an enzyme highly engineered in its function.[62,63] The EPT mechanism observed in this [NiFe] H_2ase may be different or absent in the less studied [FeFe] type of H_2ases, where again there is little thermodynamic overpotential, but a significant bias toward proton reduction and substantially faster TOF.[62,64,65] In a broader sense, the combined power of separately resolving the intermolecular ET and catalytic steps developed herein could open new doors for the study of other catalysts or redox active enzymes, not only H_2ases, which have been proposed to involve complex proton-coupled redox chemistry.[5] The combinatory methodology presented herein of structure (infrared) and chemical potential (visible) specific kinetics after a phototriggered perturbation could thus be a powerful technique for the study of complex redox processes in catalytic or enzymatic systems.

(2). Ni_a-C to Ni_a-SR Transition. The second proton associated reduction event in the catalytic cycle, the Ni_a-C reduction to Ni_a-SR, was also investigated at various pH's and solvent isotope compositions. Here the kinetics of active site chemistry are similar to the overall TOF; thus, the steady state kinetics may reflect aspects of the elementary details of this process. The reduction of Ni_a-C was observed to be pH independent in pre-steady state kinetics (Figure 6). Conversely. the Ni_a-SR formation was pH dependent with nearly the same slope as the pD dependence of the Ni_a-C formation. In contrast to the Ni_a-S reduction, this process is instead consistent with a stepwise ET-PT mechanism, and an intermediate is inferred based on the delay of Ni_a-SR formation. The data were not described well by a coupled model (Supporting Information Figure S6, Table S4) further validating the stepwise mechanism. Reduction of Ni_a-C results in the formation of a transient state we term Ni_a-SR^-, a presumably EPR silent species. A small observed KIE in H_2O vs D_2O of Ni_a-C decay (1.2) at pH(D) 7.0 is consistent with this interpretation as an ET modulated process (Supporting Information Table S3). No KIE was observed for the Ni_a-SR formation. This is again somewhat intuitive since the trivalent nickel site would appear to favor direct reduction followed by protonation rather than protonating the electron deficient Ni_a-C state. The lack of a KIE on Ni_a-SR formation could be due to a reduction induced conformational step which brings the proton into the proper orientation for PT with PT faster than the conformational step. The recently reported subatomic resolution X-ray crystal structure of the nearly homogeneously prepared Ni_a-SR form of the [NiFe] H_2ase from *D. vulgaris* Miyazaki F shows that the Ni−S bond trans to the hydride becomes elongated, which may also be involved in stabilization of this species.[28] Further experiments on this process, including temperature dependence, will help shed light on the explicit details and potentially detect the intermediate directly.

On the basis of the observed pH dependence of Ni_a-SR formation, at sufficiently low pH (<6) a PT-ET mechanism would likely be favored over the presently observed ET-PT mechanism, resulting in a trivalent protonated state we term Ni_a-D. It is unclear whether this intermediate could be trapped because PT may be fast after reduction which likely modulates the active site pK_a substantially. This would result in an inversion of the stepwise mechanism, but no intermediate formation due to a fast second step. These states, the Ni_a-D and Ni_a-SR^- and the intermediate state Ni_a-I, complete the two-dimensional (proton and electron) elementary mechanism of proton-coupled reduction of the *Pf* [NiFe] H_2ase illustrated in

DOI: 10.1021/jacs.5b01791
J. Am. Chem. Soc. 2015, 137, 4558−4566

Scheme 2. Previously Established "Standard" Model and Newly Established Elementary Model for Proton Reduction by [NiFe] H_2ases[a]

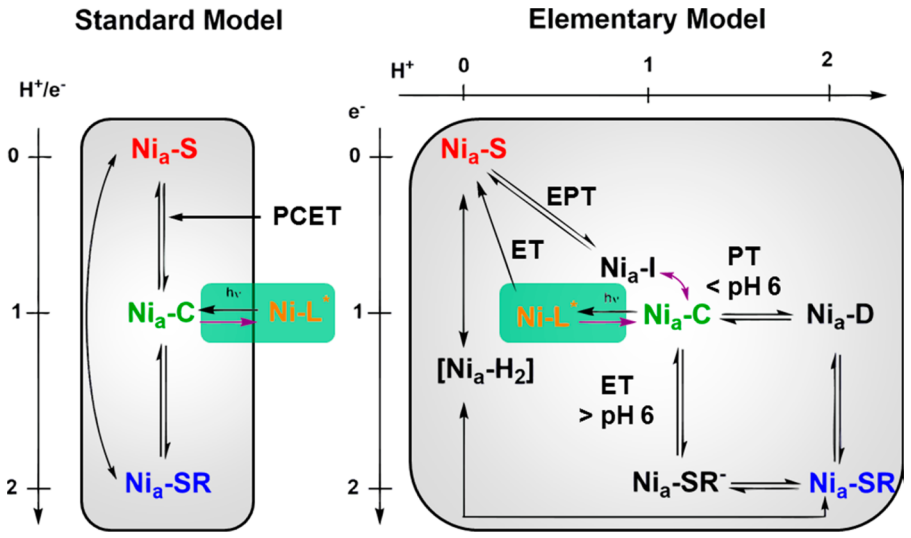

[a]Previously observed intermediates are shown in color corresponding to colors used in the main text. New proposed intermediates, as well as the debated Ni_a-H_2 state are shown in black. Ni_a-I and Ni-L, as described in the text may be very similar or identical and are formally isoelectronic and isoprotic with the Ni_a-C state; i.e., one electron reduced and mono-protonated. Purple arrows indicate hydride transfer in which no electrons or protons are exchanged to/from the active site. Ni-L is shown in green indicating a photo-chemically activated state.

Scheme 2. In this mechanism, the most oxidized catalytically active state, Ni_a-S, is reduced and protonated simultaneously in a concerted EPT process likely involving substantial proton tunneling to form the Ni_a-I state. This intermediate state rapidly transforms by hydride formation to the known Ni_a-C state, a similar, if not identical process to that observed in the reformation of Ni_a-C from the photoproduct Ni-L. Ni_a-C is converted to the most reduced catalytically active state Ni_a-SR by a stepwise ET-PT mechanism resulting in intermediate Ni_a-SR^- en route to formation of Ni_a-SR. The ET-PT mechanism of Ni_a-C reduction can be tuned by pH to bias a PT-ET mechanism which results in a different intermediate Ni_a-D. An additional state involved in the complete mechanism of H^+ reduction has been proposed involving a metal bound H_2 molecule before product release (here termed Ni_a-H_2, Scheme 2). The nature of this state and its relevance as a true intermediate or a transition state in product formation has not been established representing another challenge in the determination of the complete mechanism of these enzymes. The mechanism proposed in Scheme 2 completes the [NiFe] H^+ reduction mechanism composed entirely of elementary chemical steps.

CONCLUSION

We have reported the first ever sub-TOF investigation of interfacial ET and active site chemistry on a [NiFe] H_2ase. Rapid initiation and fast detection by nanosecond transient infrared absorbance spectroscopy enable the observation of active site chemistry beyond the rate-determining step. Active site dynamics for the three proposed reaction intermediates were observed faster than the overall TOF, establishing their kinetic competency for the first time. Furthermore, the pre-steady state dynamics revealed three distinct mechanism of proton-coupled electron transfer in proton reduction, EPT, PT-ET and ET-PT, all modulated by the protein environment and experimental conditions. Similar multisite EPT processes have been implicated in numerous enzymes including ribonucleotide reductase, photosystem II and cytochrome c oxidase, but have not been demonstrated explicitly. This [NiFe] H_2ase may thus be an advantageous system for elaborate studies on structural aspects of the enzyme matrix that facilitate low barrier EPT, a feature that if rationally engineered could assist development of reversible biomimetic catalysts.

ASSOCIATED CONTENT

Supporting Information

Tables, figures and text describing the instrumental design, UV−vis analysis, chemical potential jump calculations, temperature dependent kinetics, kinetic rate tables and initial equilibrium state populations in pre-steady state kinetics. This material is available free of charge via the Internet at http://pubs.acs.org.

AUTHOR INFORMATION

Corresponding Author

*briandyer@emory.edu

Notes

The authors declare no competing financial interest.

ACKNOWLEDGMENTS

This research was supported by a grant (DE-FG05-95ER20175 to M.W.A.) from the Division of Chemical Sciences, Geosciences and Biosciences, Office of Basic Energy Sciences of the U.S. Department of Energy and by grant (DMR1409851 to R.B.D.) from the National Science Foundation.

REFERENCES

(1) Warren, J. J.; Tronic, T. A.; Mayer, J. M. *Chem. Rev.* **2010**, *110*, 6961.
(2) Weinberg, D. R.; Gagliardi, C. J.; Hull, J. F.; Murphy, C. F.; Kent, C. A.; Westlake, B. C.; Paul, A.; Ess, D. H.; McCafferty, D. G.; Meyer, T. J. *Chem. Rev.* **2012**, *112*, 4016.
(3) Hammes-Schiffer, S.; Stuchebrukhov, A. A. *Chem. Rev.* **2010**, *110*, 6939.

DOI: 10.1021/jacs.5b01791
J. Am. Chem. Soc. 2015, 137, 4558−4566

(4) Knapp, M. J.; Rickert, K.; Klinman, J. P. *J. Am. Chem. Soc.* **2002**, *124*, 3865.
(5) Reece, S. Y.; Nocera, D. G. *Annu. Rev. Biochem.* **2009**, *78*, 673.
(6) Beratan, D. N.; Liu, C.; Migliore, A.; Polizzi, N. F.; Skourtis, S. S.; Zhang, P.; Zhang, Y. *Acc. Chem. Res.* **2014**, *48*, 474.
(7) Winkler, J. R.; Gray, H. B. *Chem. Rev.* **2014**, *114*, 3369.
(8) Fontecilla-Camps, J. C.; Volbeda, A.; Cavazza, C.; Nicolet, Y. *Chem. Rev.* **2007**, *107*, 4273.
(9) Lubitz, W.; Ogata, H.; Rudiger, O.; Reijerse, E. *Chem. Rev.* **2014**, *114*, 4081.
(10) Jones, A. K.; Sillery, E.; Albracht, S. P. J.; Armstrong, F. A. *Chem. Commun.* **2002**, 866.
(11) Pershad, H. R.; Duff, J. L. C.; Heering, H. A.; Duin, E. C.; Albracht, S. P. J.; Armstrong, F. A. *Biochemistry* **1999**, *38*, 8992.
(12) Woodward, J.; Orr, M.; Cordray, K.; Greenbaum, E. *Nature* **2000**, *405*, 1014.
(13) Beer, L. L.; Boyd, E. S.; Peters, J. W.; Posewitz, M. C. *Curr. . Biotechnol.* **2009**, *20*, 264.
(14) Camara, J. M.; Rauchfuss, T. B. *Nat. Chem.* **2012**, *4*, 26.
(15) Helm, M. L.; Stewart, M. P.; Bullock, R. M.; DuBois, M. R.; DuBois, D. L. *Science* **2011**, *333*, 863.
(16) Ogo, S.; Ichikawa, K.; Kishima, T.; Matsumoto, T.; Nakai, H.; Kusaka, K.; Ohhara, T. *Science* **2013**, *339*, 682.
(17) Tard, C.; Pickett, C. J. *Chem. Rev.* **2009**, *109*, 2245.
(18) Armstrong, F. A.; Albracht, P. J. *Philos. Trans. R. Soc., A* **2005**, *363*, 937.
(19) Pandelia, M. E.; Ogata, H.; Lubitz, W. *ChemPhysChem* **2010**, *11*, 1127.
(20) George, S. J.; Kurkin, S.; Thorneley, R. N. F.; Albracht, S. P. J. *Biochemistry* **2004**, *43*, 6808.
(21) Happe, R. P.; Roseboom, W.; Albracht, S. P. J. *Eur. J. Biochem.* **1999**, *259*, 602.
(22) deLacey, A. L.; Hatchikian, E. C.; Volbeda, A.; Frey, M.; FontecillaCamps, J. C.; Fernandez, V. M. *J. Am. Chem. Soc.* **1997**, *119*, 7181.
(23) DeLacey, A. L.; Stadler, C.; Fernandez, V. M.; Hatchikian, E. C.; Fan, H. J.; Li, S. H.; Hall, M. B. *J. Biol. Inorg. Chem.* **2002**, *7*, 318.
(24) Fichtner, C.; Laurich, C.; Bothe, E.; Lubitz, W. *Biochemistry* **2006**, *45*, 9706.
(25) De Lacey, A. L.; Fernandez, V. M.; Rousset, M.; Cammack, R. *Chem. Rev.* **2007**, *107*, 4304.
(26) Delgado-Jaime, M. U.; Shaafat, H.; Kramer, T.; Weber, K.; Neese, F.; Lubitz, W.; DeBeer, S.; DeBeer, S. *J. Biol. Inorg. Chem.* **2014**, *19*, S346.
(27) Hoffman, B. M.; Lukoyanov, D.; Yang, Z. H.; Dean, D. R.; Seefeldt, L. C. *Chem. Rev.* **2014**, *114*, 4041.
(28) Ogata, H.; Nishikawa, K.; Lubitz, W. *Nature* **2015**, DOI: 10.1038/nature14110.
(29) Chandrayan, S. K.; Wu, C. H.; McTernan, P. M.; Adams, M. W. *Protein Expression Purif.* **2015**, *107*, 90.
(30) Bryant, F. O.; Adams, M. W. W. *J. Biol. Chem.* **1989**, *264*, 5070.
(31) van Haaster, D. J.; Silva, P. J.; Hagedoorn, P. L.; Jongejan, J. A.; Hagen, W. R. *J. Bacteriol.* **2008**, *190*, 1584.
(32) Silva, P. J.; de Castro, B.; Hagen, W. R. *J. Biol. Inorg. Chem.* **1999**, *4*, 284.
(33) Vanelp, J.; Peng, G.; Zhou, Z. H.; Adams, M. W. W.; Baidya, N.; Mascharak, P. K.; Cramer, S. P. *Inorg. Chem.* **1995**, *34*, 2501.
(34) Wang, H. X.; Ralston, C. Y.; Patil, D. S.; Jones, R. M.; Gu, W.; Verhagen, M.; Adams, M.; Ge, P.; Riordan, C.; Marganian, C. A.; Mascharak, P.; Kovacs, J.; Miller, C. G.; Collins, T. J.; Brooker, S.; Croucher, P. D.; Wang, K.; Stiefel, E. I.; Cramer, S. P. *J. Am. Chem. Soc.* **2000**, *122*, 10544.
(35) Silva, P. J.; Amorim, M. J.; Hagedoorn, P. L.; Wassink, H.; Haaker, H.; Hagen, W. R. *J. Inorg. Biochem.* **1999**, *74*, 297.
(36) Bagley, K. A.; Duin, E. C.; Roseboom, W.; Albracht, S. P. J.; Woodruff, W. H. *Biochemistry* **1995**, *34*, 5527.
(37) Czochralska, B.; Lindqvist, L. *Chem. Phys. Lett.* **1983**, *101*, 297.
(38) Lindqvist, L.; Czochralska, B.; Grigorov, I. *Chem. Phys. Lett.* **1985**, *119*, 494.
(39) Orii, Y. *Biochemistry* **1993**, *32*, 11910.
(40) Tai, H.; Nishikawa, K.; Suzuki, M.; Higuchi, Y.; Hirota, S. *Angew. Chem.* **2014**, *53*, 13817.
(41) Vanderzwaan, J. W.; Albracht, S. P. J.; Fontijn, R. D.; Slater, E. C. *FEBS Lett.* **1985**, *179*, 271.
(42) Kellers, P.; Pandelia, M. E.; Currell, L. J.; Gorner, H.; Lubitz, W. *Phys. Chem. Chem. Phys.* **2009**, *11*, 8680.
(43) Foerster, S.; Stein, M.; Brecht, M.; Ogata, H.; Higuchi, Y.; Lubitz, W. *J. Am. Chem. Soc.* **2003**, *125*, 83.
(44) Pandelia, M. E.; Infossi, P.; Stein, M.; Giudici-Orticoni, M. T.; Lubitz, W. *Chem. Commun.* **2012**, *48*, 823.
(45) Saggu, M.; Zebger, I.; Ludwig, M.; Lenz, O.; Friedrich, B.; Hildebrandt, P.; Lendzian, F. *J. Biol. Chem.* **2009**, *284*, 16264.
(46) Brecht, M.; van Gastel, M.; Buhrke, T.; Friedrich, B.; Lubitz, W. *J. Am. Chem. Soc.* **2003**, *125*, 13075.
(47) Foerster, S.; van Gastel, M.; Brecht, M.; Lubitz, W. *J. Biol. Inorg. Chem.* **2005**, *10*, 51.
(48) Jiang, G. J.; Person, W. B.; Brown, K. G. *J. Chem. Phys.* **1975**, *62*, 1201.
(49) Alben, J. O.; Moh, P. P.; Fiamingo, F. G.; Altschuld, R. A. *Proc. Natl. Acad. Sci. U.S.A.* **1981**, *78*, 234.
(50) Glickman, M. H.; Klinman, J. P. *Biochemistry* **1996**, *35*, 12882.
(51) Jonsson, T.; Glickman, M. H.; Sun, S. J.; Klinman, J. P. *J. Am. Chem. Soc.* **1996**, *118*, 10319.
(52) Pardo, A.; De Lacey, A. L.; Fernandez, V. M.; Fan, H. J.; Fan, Y.; Hall, M. B. *J. Biol. Inorg. Chem.* **2006**, *11*, 286.
(53) Siegbahn, P. E.; Tye, J. W.; Hall, M. B. *Chem. Rev.* **2007**, *107*, 4414.
(54) Lill, S. O. N.; Siegbahn, P. E. M. *Biochemistry* **2009**, *48*, 1056.
(55) Dementin, S.; Burlat, B.; De Lacey, A. L.; Pardo, A.; Adryanczyk-Perrier, G.; Guigliarelli, B.; Fernandez, V. M.; Rousset, M. *J. Biol. Chem.* **2004**, *279*, 10508.
(56) Massanz, C.; Fliedrich, B. *Biochemistry* **1999**, *38*, 14330.
(57) Burgdorf, T.; De Lacey, A. L.; Friedrich, B. *J. Bacteriol.* **2002**, *184*, 6280.
(58) Siegbahn, P. E. M. *Adv. Inorg. Chem.* **2004**, *56*, 101.
(59) van Haaster, D. J.; Hagedoorn, P. L.; Jongejan, J. A.; Hagen, W. R. *Biochem. Soc. Trans.* **2005**, *33*, 12.
(60) Vignais, P. M.; Billoud, B. *Chem. Rev.* **2007**, *107*, 4206.
(61) Vincent, K. A.; Parkin, A.; Armstrong, F. A. *Chem. Rev.* **2007**, *107*, 4366.
(62) Hexter, S. V.; Grey, F.; Happe, T.; Climent, V.; Armstrong, F. A. *Proc. Natl. Acad. Sci. U.S.A.* **2012**, *109*, 18232.
(63) Abou Hamdan, A.; Dementin, S.; Liebgott, P. P.; Gutierrez-Sanz, O.; Richaud, P.; De Lacey, A. L.; Roussett, M.; Bertrand, P.; Cournac, L.; Leger, C. *J. Am. Chem. Soc.* **2012**, *134*, 8368.
(64) Madden, C.; Vaughn, M. D.; Diez-Perez, I.; Brown, K. A.; King, P. W.; Gust, D.; Moore, A. L.; Moore, T. A. *J. Am. Chem. Soc.* **2012**, *134*, 1577.
(65) Parkin, A.; Cavazza, C.; Fontecilla-Camps, J. C.; Armstrong, F. A. *J. Am. Chem. Soc.* **2006**, *128*, 16808.

DOI: 10.1021/jacs.5b01791
J. Am. Chem. Soc. 2015, 137, 4558−4566